Journal of Translational Medicine

RESEARCH

Open Access

Glioblastoma resistance to EGFR antibody-drug conjugate is driven by transcriptional reprogramming and TEK-induced EGFR suppression

Mylan R. Blomquist[1,2,3,4†], Teresa M. R. Noviello[5,6†], Christopher Sereduk[1,2], Dustin Grief[1,2,4], Francesca P. Caruso[7], Ritin Sharma[8,9], Krystine Garcia-Mansfield[8], Patrick Pirrotte[8,9], Jean Kloss[1], Fulvio D'Angelo[10], Bianca M. Marin[11], Kendra Porath[11], Sonia Jain[11], Benjamin Rabichow[4], Shannon P. Fortin Ensign[1,12], Antonio Iavarone[6,10], Antonella Paladino[13], Jann N. Sarkaria[11], Joseph C. Loftus[1], Michele Ceccarelli[5,6*] and Nhan L. Tran[1,2*]

Abstract

Background Glioblastoma (GBM), the most common primary malignant brain tumor in adults, remains uniformly fatal due to the lack of effective targeted therapies. The epidermal growth factor receptor (EGFR) is the most frequently altered receptor tyrosine kinase oncogene in GBM with most alterations impacting the receptor ectodomain function, including gene amplification, mutation, rearrangement, and splicing site changes, which occur in approximately 50% of GBM tumors. Depatuxizumab mafodotin (Depatux-M; ABT-414), an antibody-drug conjugate composed of an EGFR-specific antibody (ABT-806) that recognizes the EGFR ectodomain linked to the cytotoxic agent monomethyl auristatin F, initially showed clinical promise. However, it failed to improve survival in phase III trials, highlighting an urgent need to understand mechanisms of resistance.

Methods We generated in vivo ABT-414 resistant GBM models using patient-derived xenografts (PDXs) and performed genomics and transcriptomic profiling, including whole exome sequencing, bulk RNA sequencing, and single-cell RNA sequencing.

Results ABT-414-resistant tumors exhibited transcriptional reprogramming characterized by upregulation of synaptic and developmental gene networks and downregulation of biosynthetic processes, indicative of a plastic, therapy-adaptive state. Whole-exome sequencing revealed novel mutations exclusive to resistant tumors, including a recurrent TEK (TIE2) S466I point mutation present in all ABT-414 resistant GBM12 PDX tumors. Functional validation

[†]Mylan R. Blomquist and Teresa M.R. Noviello contributed equally to this work.

*Correspondence:
Michele Ceccarelli
mxc2982@miami.edu
Nhan L. Tran
tran.nhan@mayo.edu

Full list of author information is available at the end of the article

demonstrated that ectopic expression of TEK S466I and TEK WT in PDX models reduced EGFR levels, suggesting a novel feedback mechanism linking TEK signaling to EGFR downregulation and contributes to resistance.

Conclusion Our findings demonstrate that resistance to ABT-414 arises through both adaptive transcriptional remodeling and newly acquired genetic alterations. TEK-mediated suppression of EGFR represents a previously unrecognized mechanism of resistance, with potential implications for overcoming antibody-drug conjugate failure in GBM.

Keywords Glioblastoma, EGFR, Resistance, Antibody drug conjugate

Introduction

Glioblastoma remains an incurable disease due in part to its extensive intratumoral heterogeneity and rapid development of treatment resistance, rendering targeted therapies ineffective to date [1, 2]. While other malignancies are increasingly treated with targeted inhibitors, the first line of care for GBM has remained largely unchanged in over 20 years, consisting of maximum safe surgical resection, temozolomide, and radiation [3]. Epidermal growth factor receptor (EGFR) is an attractive therapeutic target in several malignancies, including GBM, due to its role in oncogenesis and cell proliferation. Genomic amplification is the most commonly seen EGFR alteration in GBM occurring in 40–60% of primary tumors, with nearly half of these also expressing EGFRvIII, a constitutively active, truncated variant of EGFR, followed by less common alterations including missense mutations [4]. However, despite the high frequency of altered EGFR in GBM, EGFR inhibition has thus far not improved patient overall survival. Almost all *EGFR* alterations in GBM occur in the extracellular domain, with individual tumors often harboring multiple unique EGFR alterations concurrently, which can limit the effectiveness of EGFR tyrosine kinase inhibitors [5–8]. In contrast to the direct inhibition of EGFR kinase activity, antibody-drug conjugates (ADC) bind extracellularly, taking advantage of the high expression of oncogenic EGFR on the GBM cell surface. Point mutations, exon variants, and amplification all alter the conformation of the extracellular domain of EGFR to structurally reveal a cryptic epitope exposed in the transition from inactive to active receptor state and not otherwise exposed in wild-type EGFR [9], making this extracellular domain an attractive target in GBM by conferring the potential for cytotoxicity selective for the many EGFR alterations seen in GBM. ABT-806 is a monoclonal antibody that recognizes this cryptic epitope, and Depatuxizumab-mafodotin (Depatux-M; ABT-414) is a 148.3 kDa ADC that targets EGFR using ABT-806 conjugated to anti-tubulin agent monomethyl auristatin F (MMAF). Following receptor binding, ABT414 is internalized and trafficked to the lysosome, where the maleimidocaproyl linker between MMAF and the antibody is degraded, releasing MMAF into the cell to disrupt microtubule polymerization and induce cell death. Due to a negative charge on the degradation product, MMAF cannot cross biological membranes, rendering ABT-414 unable to exert bystander effect on nearby cancer cells, but by the same merit less likely to exert cytotoxicity on nearby healthy immune cells, neurons, and glia [10–12]. While ABT-414 showed strong preclinical efficacy and advanced through Phase I and Phase II trials, it failed to improve survival in both newly diagnosed and recurrent GBM in a Phase III trial [13]. ABT-414 remains the most advanced ADC tested in GBM, yet the mechanisms underlying resistance to this therapeutic class are poorly understood, particularly when compared to well-studied resistance mechanisms against EGFR small molecule inhibitors. The current body of evidence demonstrates that loss of target expression drives resistance to ABT-414 [14] and other, well-studied ADCs, such as trastuzumab emtansine [15]. However, the mechanism of target downregulation remains unclear. The complex extra- and intracellular processes required for ADCs to induce cytotoxicity, including antigen recognition, internalization, and intracellular processing and degradation, provide several opportunities for emergent resistance, rendering these drugs exceptionally difficult to study in vitro and in vivo [15]. Further, pharmacodynamic/pharmacokinetic limitations hinder this often large, bulky class of drugs, especially in CNS tumors. ABT-414 distributes heterogeneously across the blood-brain-barrier, hindering efficacy and confounding studies of resistance, as cancer cells are not uniformly exposed to the ADC [14]. Investigating the failure of ABT-414 to provide overall survival benefit in glioblastoma provides a critical opportunity to understand more about resistance to ADCs in the context of EGFR biology and assess the limitations of this strategy to improve it in the future.

This study investigates genomic and transcriptomic mechanisms driving resistance to ABT-414 in GBM. The patient-derived xenograft (PDX) GBM12 model from the Mayo Clinic Brain Tumor PDX National Resource was chosen for its previously documented capacity to acquire resistance to ABT-414 after an initial period of sensitivity [14]. We used orthotopic implantations to examine ABT-414 resistance in the context of an intact blood brain barrier and heterogeneous drug distribution, and heterotopic implantations to assess resistance under the

conditions of a more uniform drug biodistribution. Mice bearing GBM12 were treated with ABT-414 until tumors relapsed, at which point tumors were harvested and subject to whole exome, bulk RNA, and single cell RNA sequencing.

Transcriptional analyses revealed marked reprogramming in ABT-414-resistant intracranial tumors, characterized by upregulation of genes associated with neurodevelopment and synaptic signaling, and a downregulation of pathways involved in macromolecule biosynthesis. Notably, the resistant intracranial tumors showed increased expression of ID proteins ID1 and ID3, previously associated with a drug-resistant phenotype and maintenance of self-renewal capacity in GBM [16–18]. Heterotopic resistant tumors exhibited similar pathway enrichment, with an added increase in extracellular matrix organization, suggesting context-specific adaptations. Genomic profiling identified a recurrent *de novo* mutation in the angiopoietin receptor *TEK* (TIE2) absent from the parent GBM12 tumor. Functional validation revealed that TEK protein, both wild-type and mutant (S466I), drives downregulation of EGFR, providing mechanistic insight into the loss of EGFR expression observed in ABT-414 resistance [14]. These findings highlight dual mechanisms of resistance involving both adaptive transcriptional plasticity and selection for novel genetic variants that bypass ADC-mediated cytotoxicity.

Results

Induction of acquired resistance to ABT-414 in GBM12

GBM12 is a primary, *IDH*-wild type glioblastoma harboring *EGFR* amplification and the *EGFR* G719A point mutation, previously characterized within the Mayo Clinic Brain Tumor PDX National Resource [19]. To model acquired resistance to ABT-414, luciferase-expressing GBM12 cells were implanted into athymic nude mice either orthotopically (intracranially) or heterotopically (subcutaneously in the flank). Tumor establishment was confirmed by bioluminescence imaging, after which mice were randomized to receive AB095 (isotype control), ABT-806 (parental EGFR antibody), or ABT-414 (Fig. 1A). As previously reported [14], ABT-414 treatment resulted in the initial tumor remission followed by recurrence. In both intracranial (Fig. 1B) and flank (Fig. 1C) models, ABT-414 significantly prolonged survival compared to AB095 and ABT-806 during the initial response phase, prior to acquisition of resistance. Treatment was continued weekly throughout the study duration, allowing for longitudinal assessment of tumor response dynamics and resistance acquisition.

ABT-414 resistant GBM12 exhibits upregulation of synaptic signaling, tissue development, and ID family transcripts

To identify pathways associated with acquired ABT-414 resistance, we analyzed differentially expressed genes in ABT-414-resistant GBM12 tumors compared to tumors treated with control antibodies AB095 or ABT-806. In the orthotopic intracranial model (Figs. 2A, 2B), resistant tumors show significant upregulation of genes involved in synaptic signaling and neural tissue development. Enriched pathways included synaptic transmission, membrane potential regulation, glutamate signaling, synapse organization, embryonic organ morphogenesis, forebrain development, response to bone morphogenetic protein (BMP) signaling, and mesenchyme development. Notably, *ID1* and *ID3* transcripts were among the most highly upregulated (Fig. 2A). These ID family proteins have been implicated in maintaining the glioma stem cell niche [16]. ID1 specifically is associated with tumor recurrence and therapeutic resistance [20]. Immunoblot analysis confirmed increased protein expression of ID1 and ID3 in resistant GBM12 tumor from the flank model (Supplementary Figure S1A). In contrast, the transcripts enriched in AB095 and ABT-806 control-treated tumors were predominantly involved in metabolic and biosynthetic pathways, suggesting that ABT-414-resistant tumors may adopt a less metabolically active state (Fig. 2B).

In the heterotopic flank model (Figs. 2C, D), ABT-414 resistant tumors recapitulated several transcriptional features observed in intracranial tumors, including genes involved in development and synapse organization. However, the most significantly enriched transcripts in the resistant flank tumors were associated with extracellular matrix organization, potentially reflecting adaptations to the distinct physical constraints of the subcutaneous microenvironment. In contrast to the intracranial model, where control enriched genes were mostly involved in biosynthesis, flank control tumors (Figs. 2C, D) displayed enrichment across more diverse biological pathways (Fig. 2D).

Single cell transcriptome analysis of ABT-414 resistant GBM12 reveals upregulation of DNA replication pathways

To complement the bulk RNA sequencing and gain deeper resolution into cell-type-specific changes associated with ABT-414 resistance, we performed scRNA-seq on the tumor cohorts described above, yielding a total of 8,431 single cells. UMAP dimensionality reduction (Figs. 3A and 3B) visualizes clustering by tumor location (intracranial vs. flank) and treatment group, respectively. ABT-414-treated cells formed a distinct cluster, clearly separated from those treated with control antibodies AB095 or ABT-806. While ABT-806-treated cells largely overlap with AB095, indicating a similar transcriptional

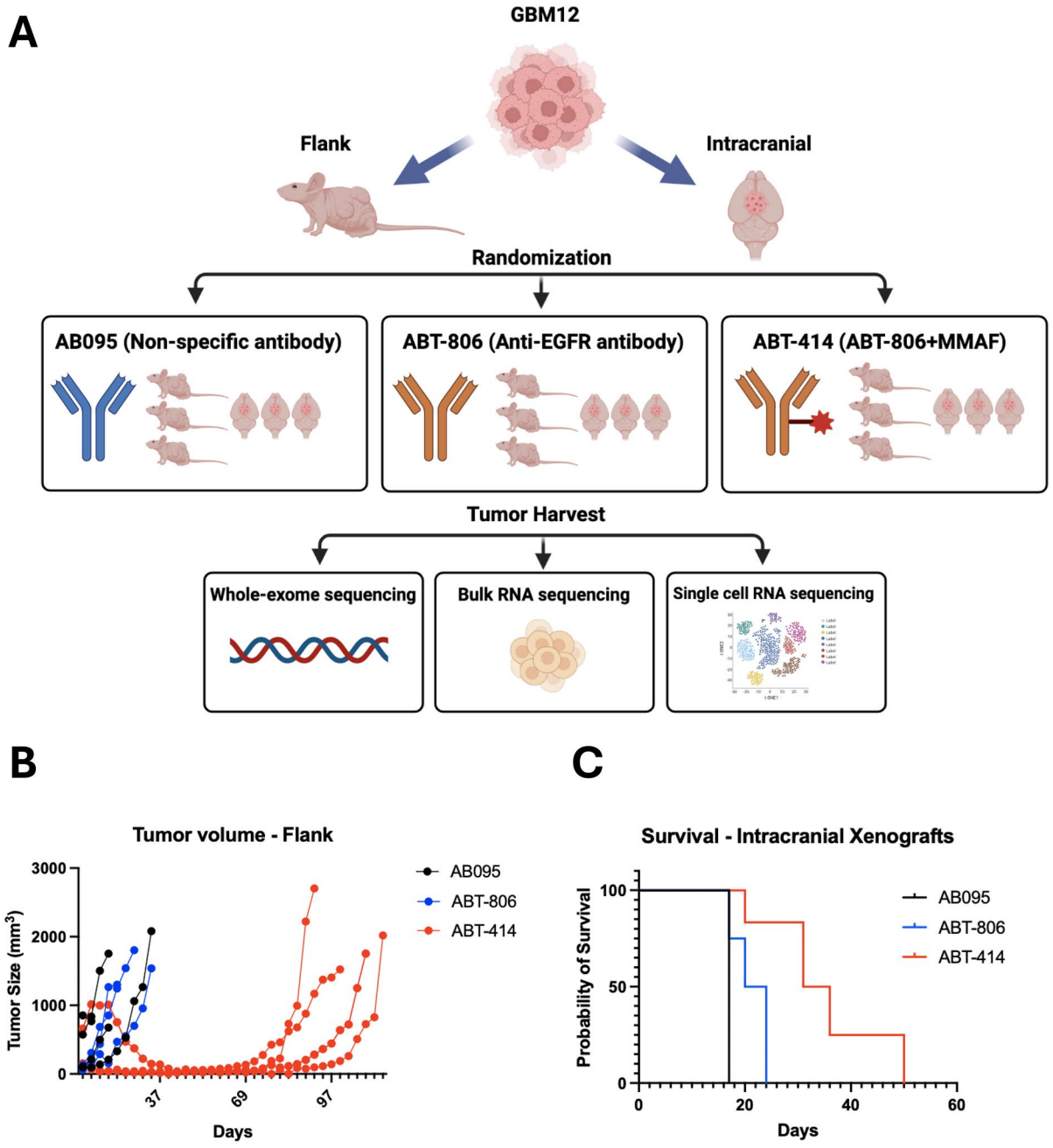

Fig. 1 Outline of experimental design. **A**. GBM12 was implanted either orthotopically (intracranial injection) or subcutaneously in the flank of athymic nude mice. Mice were randomized to AB095 (5 mg/kg), ABT-806 (10 mg/kg), or ABT-414 (5 mg/kg). Animals were treated weekly until humane endpoint was reached. Tumors were harvested at the time of animal euthanasia. **B**. Volume of GBM12 flank tumors (y axis) vs. days from the initiation of treatment (x axis) ($p < 0.001$, AB095 vs ABT-414; $p < 0.001$, ABT-806 vs ABT-414). **C**. Kaplan Meier plot showing animal survival in each treatment group in days ($p < 0.001$, AB095 vs ABT-414; $p < 0.05$ ABT806 vs ABT-414)

profile, a unique transcriptional signature was observed exclusively in a subset of AB095 treated cells. Notably, ABT-414-M-treated tumors were mapped on two different cellular subpopulations (Fig. 3B), possibly corresponding to the intracranial vs. flank tumor locations. Further analysis showed that these two populations have a very distinct transcriptional profile and fell into the same cluster (cluster 6, Supplementary Figure S1B, left), suggesting that they are significantly different from the untreated control cells. Then, we asked if these two subpopulations were genomically distinct. We used SCEVAN [21] to identify subclones and observed four different Copy Number clones, with the ABT-414-treated

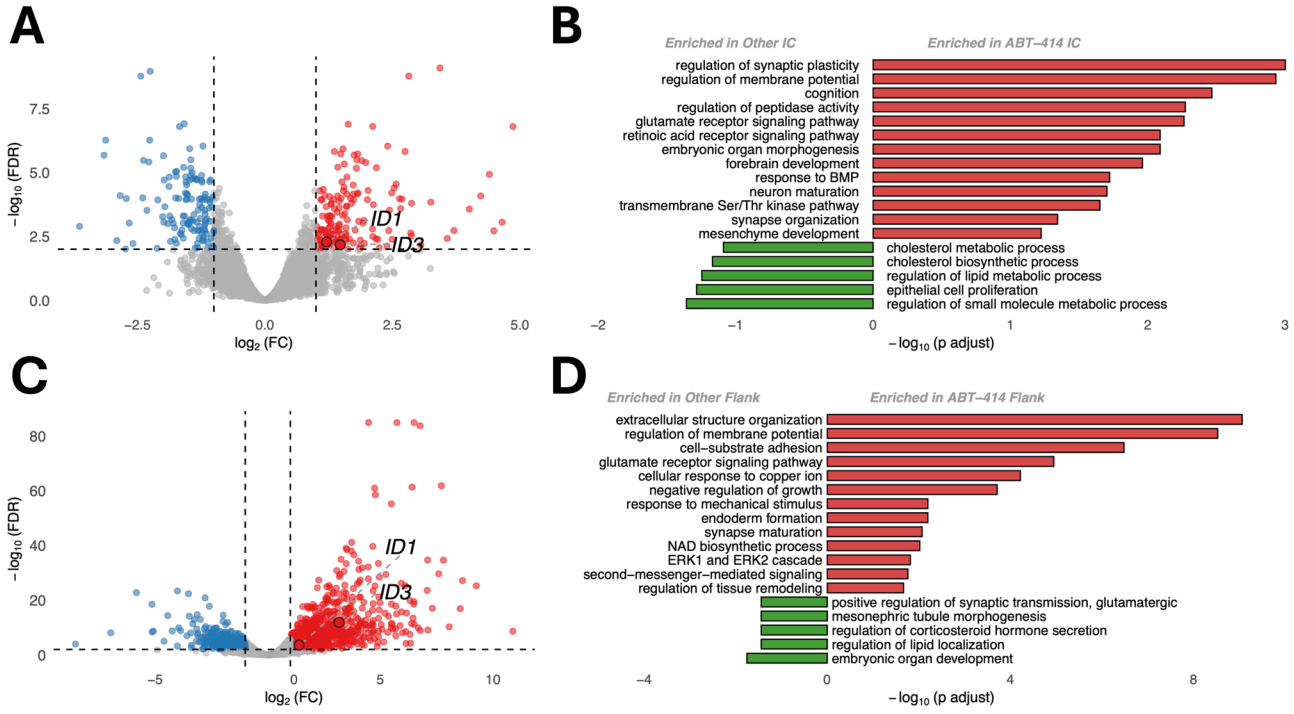

Fig. 2 Bulk-RNA-seq of ABT-414-resistant GBM12 tumors demonstrates upregulation of developmental pathways and downregulation of metabolism. **A**. Volcano plot of differentially expressed genes between ABT414 intracranial (IC) samples and other IC samples, highlighting in red significantly up-regulated genes (adjusted $p < 0.01$, $\log_2 FC \geq 0.6$) and in blue significantly down-regulated genes (adjusted $p < 0.01$, $\log_2 FC \leq -0.6$). **B**. Bar plot of -$\log_{10}$ (adjusted *p* value) for selected gene ontology categories from overrepresentation analysis, based on the comparison between ABT414 IC samples and all other IC samples. **C**. Volcano plot of differentially expressed genes between ABT414 flank samples and control flank samples, using the same significance thresholds as in **A. D**. Bar plot of -$\log_{10}$ (adjusted *p* value) for selected gene ontology categories from overrepresentation analysis, based on the comparison between ABT-414–treated flank samples and control flank samples

belonging mainly to subclones one and three (Supplementary Figure S1B, right).

We also confirmed the bulk RNA seq findings, *ID1* and *ID3* transcripts were selectively upregulated in tumor cells from ABT-414 treated intracranial tumors (Fig. 3C), rather than non-malignant stromal or immune cells. To assess whether ID1/ID3 upregulation reflects a broader reactivation of glioma stemness programs, we evaluated a panel of transcription factors known to regulate glioma stem cell self-renewal [22] in single-cell transcripts of resistant tumors. However, unlike ID1/ID3, these stemness-associated transcription factors were not enriched in ABT-414 treated tumors (Supplementary Figure S1C), suggesting that ID1/ID3 upregulation may represent a selective upregulation rather than global stem cell reprogramming.

EGFR transcripts were downregulated in resistant tumor cells, consistent with a shift away from EGFR signaling dependency under therapeutic pressure. Pathway enrichment analysis of the scRNA-seq data revealed that ABT-414-resistant intracranial tumor cells exhibited marked enrichment in DNA replication, chromosome segregation, response to ionizing radiation, ribosomal assembly, and mitochondrial function (Fig. 3D). These findings diverged from bulk RNA-seq results, which emphasized neural development and synaptic organization pathways, highlighting the distinct dimension of tumor-intrinsic biology captured by scRNA seq analysis not discernible in bulk measurements. In contrast, cells from AB095- and ABT-806-treated tumors were enriched for cholesterol and lipid metabolism pathways, in line with bulk RNAseq data showing relatively increased metabolic activity in control-treated tumors compared to resistant tumors. Analysis of resistant tumors in the heterotopic flank model confirmed these trends (Figs. 3E, F). *EGFR* transcript levels remained downregulated, and *ID3* remained upregulated in ABT-414-resistant cells (Fig. 3E). As in the intracranial model, resistant flank tumor cells exhibited enrichment for DNA replication and cell-cycle-related processes (Fig. 3F). However, the extracellular matrix remodeling signatures observed in bulk RNA-seq from flank tumors were not prominent in the single-cell analysis, suggesting this may reflect stromal rather than tumor-intrinsic changes.

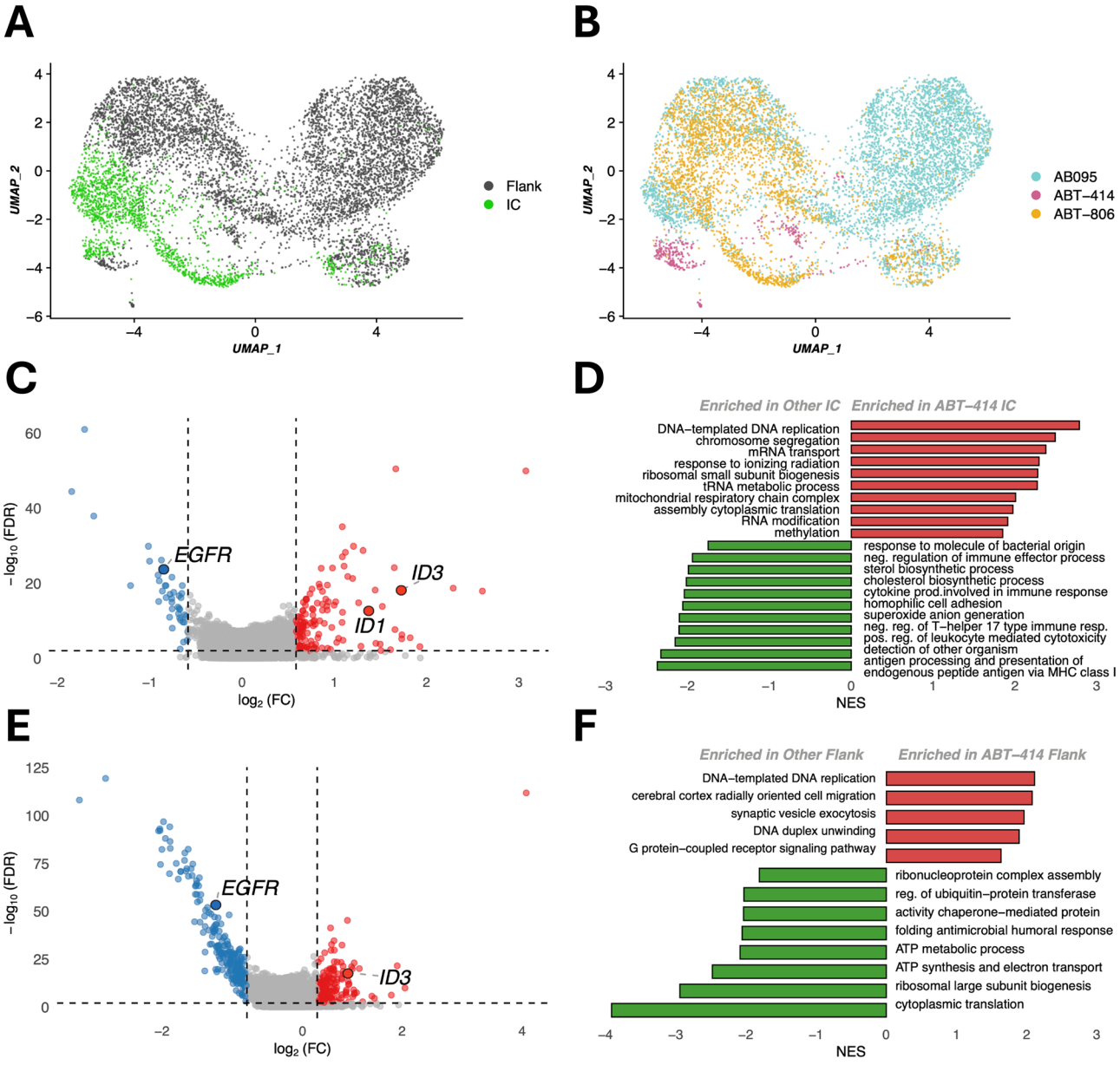

Fig. 3 Single cell RNA sequencing demonstrates adaptive resistance to ABT-414 treatment. **A**. UMAP plot of all cells based on gene expression, colored by tumor location, distinguishing intracranial (IC) tumors from flank. **B**. UMAP plot of the same cells colored by treatment group. **C**. Volcano plot of differentially expressed genes between ABT414 IC cells and all other IC cells, highlighting in red significantly up-regulated genes (adjusted $p < 0.01$, $\log_2 FC \geq 0.6$) and in blue significantly down-regulated genes (adjusted $p < 0.01$, $\log_2 FC \leq -0.6$). **D**. Bar plot of normalized enrichment scores (NES) for selected gene ontology categories from GSEA, based on the comparison between ABT414 IC cells and all other IC cells. **E**. Volcano plot of differentially expressed genes between ABT414 flank cells and all other flank cells, using the same significance thresholds as in **C**. **F**. Bar plot of NES for selected gene ontology categories from GSEA, based on the comparison between ABT414 flank cells and all other flank cells

Whole exome sequencing identified genomic alterations exclusive to ABT-414-resistant tumors

To uncover genetic mechanisms underlying acquired resistance to ABT-414, we performed whole exome sequencing on tumors from both orthotopic intracranial and flank models. Across all treatment groups, tumors retained key parental GBM12 alterations, including *TP53* mutation, *EGFR* amplification, *EGFR* G719A point mutation, and *CDKN2A* deletion, confirming consistency with the original tumor genotypes. Control-treated tumors (AB095 and ABT-806) exhibited similar patterns of somatic alteration, with no notable treatment-specific divergence (Supplementary Figure S2A). However, ABT-414-resistant tumors displayed unique *de novo* somatic alterations, including pathogenic missense variants in *HAVCR1, PLXNA2, PSD2, SRPRA*, and *TEK*, which arose

independently in each animal and were absent in all control groups (Fig. 4A).

TEK expression is associated with loss of EGFR expression and confers resistance to ABT-414

Of the somatic alterations arising only in ABT-414 resistant tumors, we focused on *TEK (*also known as *TIE2)*, given its known role in vascular remodeling and therapy resistance. This novel mutation was validated by Sanger sequencing (Supplementary Figure S3A). TEK is a transmembrane receptor tyrosine kinase activated by angiopoietin 1 and typically regulates vascular homeostasis. However, in the context of malignancy, TEK has been implicated in pathological vascular remodeling, tumor progression, and therapeutic resistance in GBM [23]. Beyond endothelial cells, TEK is also expressed on GBM tumor cells [24] and has been shown to dimerize with other receptor tyrosine kinases, such as FGFR1, to promote cell survival and resistance to PI3K inhibition [25, 26]. Given that the TEK S466I mutation lies within the extracellular FNIIIa domain, we hypothesized that this alteration may disrupt receptor interactions, including EGFR, thereby contributing to resistance to ABT-414.

To functionally test the role of TEK in modulating ABT-414 response, we stably expressed HA-tagged wild-type (WT) TEK or the TEK S466I in two PDX-derived GBM models: GBM8, which harbors endogenous EGFR amplification, and GBM22, which lacks EGFR alteration and expresses low baseline EGFR. GBM12 was not used due to poor in vitro viability. In GBM8 cells, stable expression of either WT TEK or TEK S466I resulted in a marked reduction of EGFR surface expression (Fig. 5A). Furthermore, both EGFR mRNA transcript (Fig. 5B) and protein levels (Fig. 5C) were diminished. This downregulation of EGFR corresponded with a significant decrease in sensitivity to ABT-414, indicating that TEK expression alone is sufficient to confer resistance (Fig. 5D). Similarly, in GBM22, TEK expression (WT or S466I) rendered the cells resistant to treatment (Fig. 5E). Notably, ABT-414 sensitivity was restored by overexpressing WT EGFR. However, co-expression of TEK and EGFR appeared mutually antagonistic. GBM22 cells stably expressing both constructs under identical antibiotic selection lost detectable HA-tagged TEK expression (Fig. 5F, lanes 5–6 vs. lanes 3–4), suggesting a competitive or destabilizing interaction. Due to the reproducibility of this reciprocal suppression across independent experiments, we prioritized further mechanistic studies in GBM8, where EGFR is endogenously amplified.

Proteome profiling reveals TEK S466I-induced remodeling of the kinome

Because both WT TEK and the TEK S466I mutant downregulate EGFR and confer ABT-414 resistance in vitro, we sought to determine whether the TEK S466I alteration imparts unique functional properties beyond those

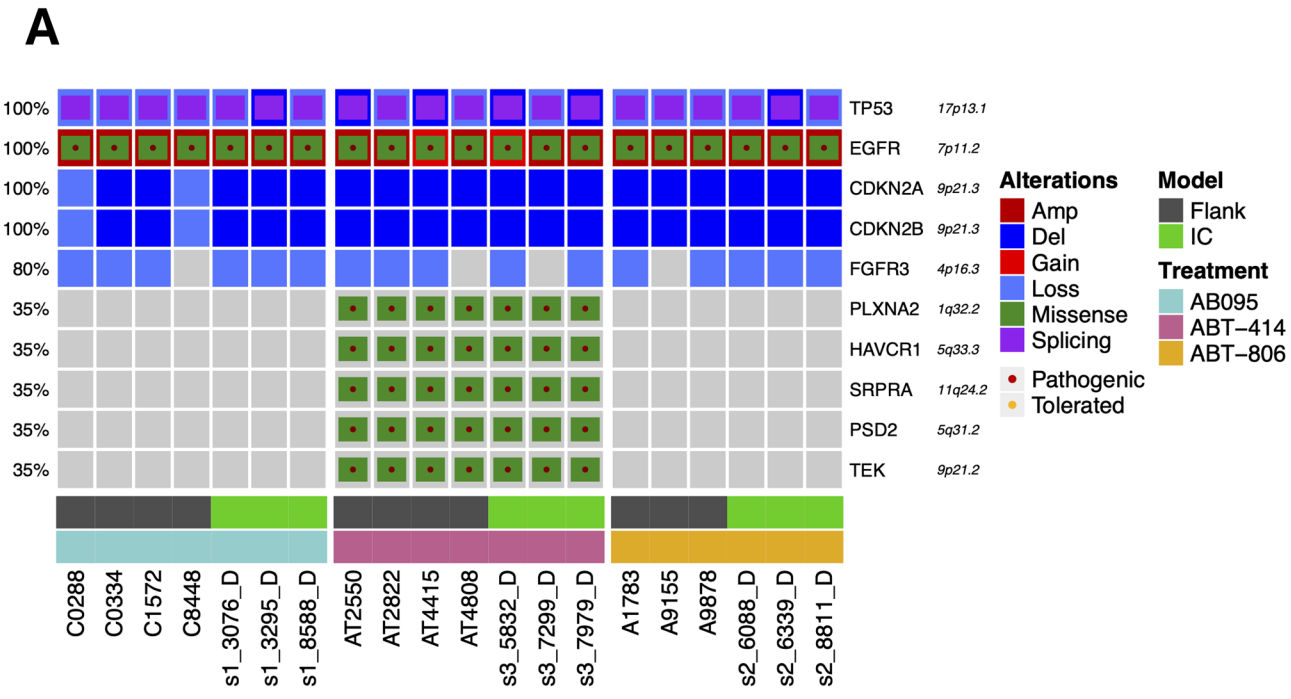

Fig. 4 Whole exome sequencing reveals somatic alterations distinct to the ABT-414-resistant tumors, specifically TEK S466I. **A**. Distinct missense mutations were detected in PLXNA2, HAVCR1, SRPRA, PSD2, and TEK in the ABT-414–treated tumors from both subcutaneous (flank) and intracranial (IC) models, highlighting genomic alterations enriched in resistant tumors

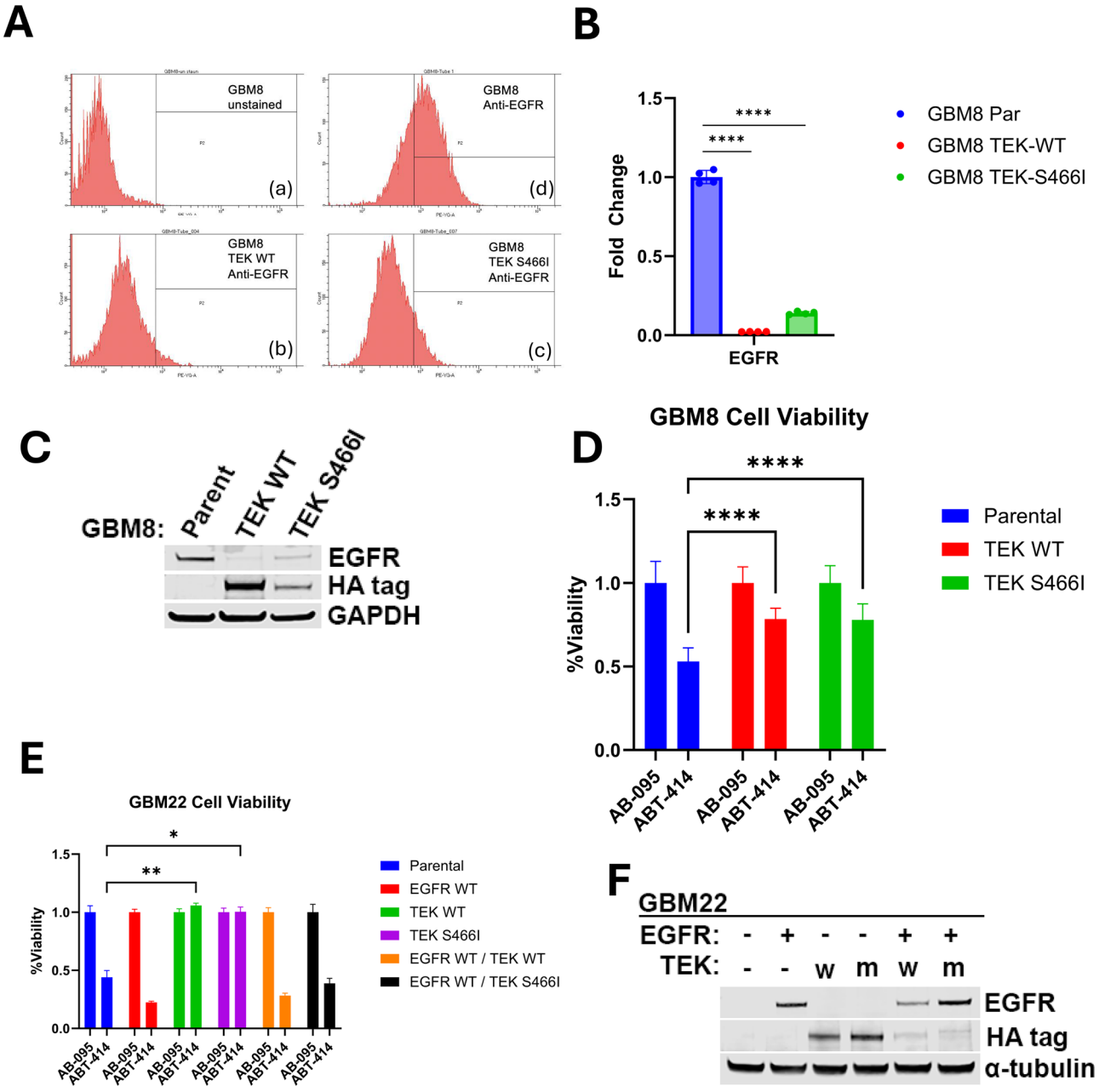

Fig. 5 TEK expression is associated with loss of EGFR expression at the RNA level and resistance to ABT-414 in vitro. **A**. Expression of TEK downregulates expression of EGFR. WT-GBM8 cells were stained with a control isotype control antibody (**a**). WT-GBM8 cells (**b**), GBM8 cells expressing WT-TEK (**c**), or GBM8 cells expressing the TEK variant S466I (**d**) were stained with a PE-conjugated anti-EGFR monoclonal antibody and EGFR expression was analyzed by flow cytometry. **B**. Gene expression level of *EGFR* for GBM8 expressing TEK-WT or TEK-S466I, assessed via qPCR. Results are shown as a fold-change compared to GBM8-parental. CT values initially normalized to 18S expression level. Error bars represent SEM and p-values represent a one-tailed t-test. **C**. Lysates of adherent GBM8 cells, either parental or stably expressing TEK WT or TEK S466I, serum starved for 24 hours immunoblotted for EGFR, HA tag, and GAPDH as a loading control. **D**. Percentage of viable GBM8 cells (cell titer glo, normalized to AB095, y axis) in each condition (x axis) X hours following treatment with 10 g/ml of ABT-414. **E**. Percentage of viable GBM22 cells (cell titer glo, normalized to AB095, y axis) in each condition (x axis) X hours following treatment with 10 g/ml of ABT-414. **F**. Lysates of adherent GBM22 cells, either parental or stably expressing TEK WT (**w**), TEK S466I (**m**), or either TEK construct plus EGFR, serum starved for 24 hours immunoblotted for EGFR, HA tag, and alpha-tubulin as a loading control

of WT receptor. To investigate whether the S466I substitution leads to structural alterations in TEK that could influence receptor function or ligand interactions, we performed in silico structural modeling and molecular dynamics simulations of the extracellular domain of TEK, focusing on the FNIIIa domain where the S466I mutation resides. The full-length structural model was built using homology-based tools (see Methods) and molecular

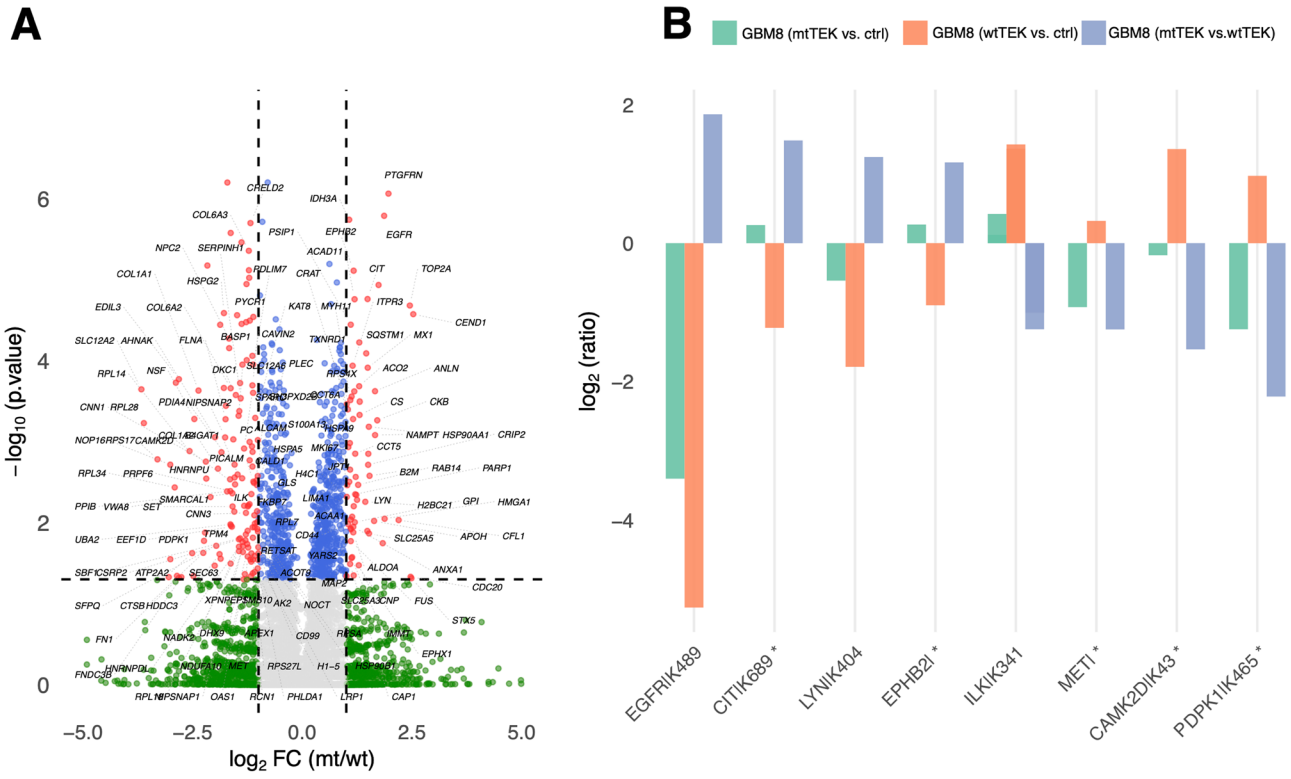

Fig. 6 Activity-based proteome profiling distinguishes downstream kinase activity in TEK S466I- and TEK WT- expressing GBM8 cells. **A**. volcano plot depicting Fold change (log_2) for each identified DBT-peptide between the mtTEK expressing GBM8 cell line and wtTEK GBM8 cell line on the x-axis and p-value ($-log_{10}$) significance from the Tukey post-hoc. Each filled circle represents a DBT-peptide. Red circles represent peptides that passed both the p-value < 0.05 and the log_2 Fold change > |1| threshold. Blue circles represent peptides that only passed the p-value < 0.05 threshold. Green circles represent peptides that only passed the log_2 Fold change > |1| threshold. Grey circles represent DBT peptides that were unchanged between the two conditions. **B**. bar plot showing log_2 Fold-change (grey bars) for kinase DBT-peptides that are significantly differentially abundant (log_2fold change > |1| and p-value < 0.05) between mtTEK and wtTEK expressing GBM8 cell line. For reference, log_2 Fold change for mtTEK vs control GBM8 cells (blue bars) and wtTEK vs control GBM8 cells (orange bars) is also shown. DBT-peptide for ILK341 is listed twice as its one peptide carries additional methionine oxidation while the other does not. For EPHB2 and MET, the modification site could not be localized on the peptide and is therefore not listed

dynamics simulations were carried out to assess protein structural stability and characterize the effect of the point mutation. The substitution of serine with isoleucine at position 466 caused a shift in FNIIIa surface electrostatic forces but did not significantly impact the overall folding or domain architecture of the TEK extracellular region. Molecular dynamic (MD)-based analyses revealed no major conformational deviations between the WT or mutant models (RMSD < 2 Å for FNIIIa), suggesting that S466I does not alter TEKs ligand-binding capacity or extracellular dimerization interface (Supplementary Figure S4A-C). Given the structural preservation, we hypothesized that the S466I mutation may instead alter intracellular signaling dynamics. To test this hypothesis, we employed activity-based proteome profiling in GBM8 cells expressing either WT TEK or TEK S466I to globally assess differential kinase activity and downstream signaling networks (Fig. 6A). Consistent with our earlier findings, EGFR kinase activity was markedly reduced in both WT TEK and TEK S466I cells relative to parental GBM8 (Fig. 6B), mirroring the transcriptional and protein expression of EGFR. However, a subset of kinases displayed divergent activity between the two TEK constructs. Specifically, CIT and EPHB2 exhibited increased kinase activity in the TEK S466I-expressing cells, whereas MET, CAMK2D, and PDPK1 activity was reduced compared to the WT TEK (Fig. 6B). Given evidence of the role of citron kinase in microtubule stabilization in glioma cells [27] and known involvement of Src family kinases and ephrin receptors in mediating cytokinesis [28], we queried whether these kinases specifically active in the TEK S466I condition confer resistance to microtubule disruption by MMAF. We found that TEK S466I GBM8 does not exhibit any increased resistance to MMAF alone (Supplementary Figure S5), suggesting that the observed kinome rewiring is not sufficient to bypass microtubule disruption directly. Together, these data support a model in which S466I may subtly modulate downstream signaling, but the primary mechanism of ABT-414 resistance in this model remains loss of EGFR, preventing efficient internalization of the antibody-drug conjugate.

Discussion

In this study, we identified both transcriptional plasticity and *de novo* genetic alterations contributing to resistance against the ADC Depatux-M/ABT-414 in orthotopic and heterotopic GBM models. Despite *EGFR* alterations being present in nearly half of GBMs, Depatux-M/ABT-414 failed to show a survival benefit in a Phase III clinical trial [13]. Prior studies attribute resistance to heterogeneous drug distribution across the blood brain barrier and loss of EGFR expression [14]. Combined with heterogenous drug distribution throughout the tumor, ABT-414 is also limited in its ability to exert bystander effect on nearby tumor cells due to the polarity of the linker-MMAF degradation product preventing its escape from the cell. Thus, the mechanism of resistance to ABT-414 depends primarily on resistance to the intact ADC rather than any component of resistance to MMAF alone as so few cells are hypothesized to be exposed to lone MMAF. In this study, we characterize the way in which drug resistance is driven by intrinsic tumor biology upon exposure to the ADC, including adaptive transcriptional and genetic changes. Our study explored ABT-414 resistance in orthotopic tumors as well as subcutaneous flank tumors to understand mechanisms of resistance outside of incomplete penetration of the drug past the blood brain barrier. Bulk RNA sequencing of resistant tumors revealed downregulation of metabolic pathways and upregulation of transcriptional programs linked to synaptic signaling and neural embryonic development, specifically increased expression of ID1 and ID3 [22]. These transcription factors are critical regulators of glioma stem maintenance [22], and in this context were upregulated in the absence of EGFR activity. Indeed, EGFR expression was lost in resistant GBM12, indicating ID1/ID3 induction can occur independently of canonical EGFR signaling [14]. While EGFR signaling has been shown to induce ID protein expression in glioblastoma [29], and reciprocally, to induce production of EGF [20], our finding suggest that resistance-associated ID1/ID3 upregulation may arise through alternative pathways, potentially indicative of a resistance response to MMAF-induced cytotoxicity directly. Complementing the bulk transcriptomic data, single-cell RNA-seq revealed enrichment of DNA replication and cell cycle programs in resistant tumor cells, suggesting an expansion of therapy-tolerant, proliferative clones. Notably, these changes were not evident in bulk profiling, underlining the importance of single-cell resolution in detecting resistance-associated cell states. Furthermore, scRNA-seq confirmed that ID1/ID3 upregulation is tumor-cell-intrinsic and not attributable to the tumor microenvironment.

Genomic profiling revealed a recurrent *de novo* mutation in the angiopoietin receptor TEK (S466I) in every resistant tumor, absent in parental tumors. Structural modeling and molecular dynamics simulation indicated that S466I does not disrupt the extracellular conformation of TEK, pointing instead to intracellular signaling changes. In fact, proteome kinase activity profiling revealed distinct signaling differences between WT TEK and the S466I variant, though these were not sufficient to bypass MMAF-induced cytotoxicity directly, suggesting that the primary resistance mechanism to ABT-414 remains EGFR downregulation. Indeed, overexpression of either WT TEK or TEK S466I in PDX cell lines resulted in loss of EGFR at the transcript and protein level and conferred resistance to ABT-414, pointing to a novel, previously undescribed link between TEK and EGFR. Despite attempts, co-immunoprecipitation of EGFR and TEK was unsuccessful, likely due to mutual exclusivity of their expression, leaving open questions about whether this relationship is direct, complex-mediated, or involved in downstream signaling affecting protein stability or trafficking. While the emergence of TEK S466I was observed in only one PDX model, the consistent appearance across multiple independent tumors supports a functional role in resistance. Further studies are needed to determine if similar TEK alterations arise in other PDX models or in patient tumors treated with anti-EGFR ADCs. Although molecular dynamics showed that TEK S466I does not significantly alter extracellular domain conformation, its recurrent emergence suggests a selective advantage, possibly through enhanced kinase activity or altered scaffolding of intracellular effectors (e.g., citron kinase, Lyn). The mutation's location in the FNIIIa domain hints at ligand-independent effect. Future work could compare phosphoproteomes of WT vs. S466I TEK to identify mutation-specific substrates.

Established mechanisms of adaptive resistance to EGFR inhibition in GBM include compensatory activation of common altered signaling pathways, such as PI3K, by alternative RTKs, with elevated activity of MET and PDGFRB well documented [30, 31]. The discovery of a TEK-mediated suppression of EGFR adds a new dimension to the understanding of resistance mechanisms in GBM and may extend to other EGFR-targeted therapies, including tyrosine kinase inhibitors and monoclonal antibodies. TEK has not previously been implicated in EGFR regulation in glioma or other cancers, and the mutual exclusivity of their expression in this context suggests a regulatory circuit with therapeutic implications. Thus, it remains unclear whether TEK-mediated EGFR suppression requires TEK kinase activity or downstream signaling mediators. Regardless, if EGFR downregulation depends on TEK kinase activity, selective TEK inhibitors [32] could be co-administered with Depatux-M/ABT414 to preserve EGFR expression and enhance EGFR-targeted ADC cytotoxicity. Moreover, central nervous system penetrant multi-TKI inhibitors that target multiple

known EGFR resistance pathways concurrently, such as Cabozantinib (RET, MET, VEGFR-1, −2 and −3, KIT, TRKB, FLT-3, AXL, ROS1, TYRO3, MER, and TEK/TIE-2 inhibition) [33–37], Regorafenib (BRAF, FGFR, KIT, PDGFR, RET, TEK, and VEGFR inhibition) [38–40], Vandetanib (EGFR, PDGFR, RET, SRC, TEK, VEGFR) [41, 42] or others, may prove even more effective at delaying or preventing resistance when co-administered with ABT-414. Thus, combination approaches targeting anticipated resistance mechanisms may offer a novel therapeutic strategy to enhance the efficacy of EGFR-ADCs in GBM.

Conclusion

In conclusion, our study identifies both transcriptional plasticity and a role for TEK as key contributors to resistance against the EGFR-targeted antibody-drug conjugate, ABT414 (Depatuxizumab mafodotin) in GBM. TEK overexpression suppresses EGFR expression and promotes resistance, revealing a previously unrecognized regulatory axis with therapeutic implications. These findings suggest that co-targeting TEK or use of multi-kinase inhibitors may enhance the efficacy of EGFR-directed therapies in GBM.

Methods

Animal studies

Culturing and propagating Mayo GBM PDXs have been extensively described [19]. All animal studies were conducted according to the Mayo Institutional Animal Care and Use Committee (IACUC). Subcutaneous tumors were established in athymic mice (Envigo) with 2×10^6 to 1×10^6 cells suspended in a 1:1 Matrigel-PBS mixture. Tumor size was measured thrice weekly. Mice were randomized and treated with an isotype control antibody AB095 (10 mg/kg), ABT-806 (10 mg/kg), or ABT-414 (5 mg/kg) intraperitoneally once a week until moribund for six months. Individual mice were euthanized after exceeding tumor measurements of 1500 mm^3 twice consecutively, 2000 mm^3 once, or other serious clinical illness, as allowed by the Mayo Clinic IACUC guidelines. Where indicated, recurrent tumors were fresh-frozen, cryopreserved and/or fresh cells were used to establish short-term explant cultures or passaged heterotopically into mice. Recurrent tumors are identified with a 'R' and the mouse number the cells originated from.

Orthotopic tumors were established as described previously [43]. Tumor growth was monitored using bioluminescence imaging (BLI). Mice were stratified by BLI signal, randomized into groups, and treated with AB095 (5 mg/kg), ABT-806 (10 mg/kg), or ABT-414 (5 mg/kg) intraperitoneally once a week. Mice with orthotopic tumors were observed daily and euthanized upon reaching a moribund state.

Whole exome sequencing (WES) analysis

Quality control of WES was performed on raw data using fastQC (v. 0.11.8) (https://www.bioinformatics.babraham.ac.uk/projects/fastqc/). Before alignment to the human genome, sequencing reads from PDX tumors were processed with Xenome [44] to classify them as human, mouse, or ambiguous. Only reads classified as human were retained and aligned to the Human reference genome (UCSC genome assembly GRCh37/hg19) using Burrows-Wheeler Aligner [45], and then processed by GATK [46] for discarding low mapping quality reads and performing indel realignment.

Somatic single-nucleotide variants (SNVs) and indels calling were performed using Sentieon Genomic Tool v. 201,911 [47]. Somatic SNVs and indels were identified by integrating the results from 6 algorithms for variants calling: Freebayes [48], MuTect2 [49], TNhaplotyper [47], TNscope [47], TNsnv [47], and VarScan2 [50].

Putative false positive variant calls were removed based on the following criteria: (i) the variant-supporting read count greater than 2; (ii) variant allele frequency greater than 0.05; (iii) average variant position in variant-supporting reads (relative to read length) > 0.1 and lower than 0.9; (iv) average distance to effective 3′ end of variant position in variant-supporting reads (relative to read length) greater than 0.2; (v) fraction of variant-supporting reads from each strand > 0.01; (vi) average mismatch quality difference (variant—reference) lower than 50; vii) average mapping quality difference (reference—variant) lower than 50. Annotation of SNVs and indels was performed using AnnoVar [51] and SnpEff [52]. The functional effect of missense SNVs and in-frame indels was computed using Polyphen2 [53], SIFT [54], and PROVEAN [55] algorithms and variants predicted as damaging at least two of them were classified as pathogenic mutations. Somatic copy number was estimated from WES reads by CNVkit [56] and GISTIC [57] was applied for identifying genomic regions recurrently amplified or deleted.

Total RNA sequencing analysis

Before alignment to the human genome, sequencing reads from PDX tumors were processed with Xenome [44] to classify them as human, mouse, or ambiguous. Only reads classified as human were retained and aligned to the human genome (UCSC genome assembly GRCh37) using STAR (v2.7.0b) [58]. Gene-level expression quantification was performed using featureCounts (v1.6.3) [59], a count-based estimation algorithm.

Downstream analyses were conducted in the R statistical environment. Raw counts were normalized to account for sample-specific GC-content biases using the EDASeq package (v2.22.0) [60]. Differential expression analysis was carried out using the edgeR package (v3.30.3) [61].

Genes with an adjusted p-value ≤0.01 (Benjamini–Hochberg correction) and an absolute log2 fold change ≥1 were considered significantly differentially expressed.

Enrichment analysis for Biological Processes was performed on differentially expressed genes (DEGs) using the clusterProfiler package (v3.3.6) [61].

Single cell RNA sequencing analysis

Sequencing reads obtained from PDX tumors were first processed using Xenocell version 1.0 [62] to categorize them as human, mouse, or ambiguous. Reads identified as human were retained for downstream analysis. The data were then processed using the 10x Genomics Cell Ranger pipeline (v3.0.2), with alignment performed against the GRCh37 human reference genome (refdata-cellranger-hg19-3.0.0). The resulting raw RNA count matrix was further analyzed using the Seurat package in R (v5.1.0) [63]. Standard quality control filters were applied to remove low-quality cells, including those with fewer than 600 or more than 7,000 detected genes, mitochondrial gene content exceeding 10% (indicative of stressed or dying cells), or total transcript counts (nCount) greater than 60,000. After filtering, 8,431 high-quality cells were retained for downstream analysis. Gene expression values were log2-transformed, and principal component analysis (PCA) was conducted using the top 2,000 most variable genes. Cellular heterogeneity was visualized using Uniform Manifold Approximation and Projection (UMAP) based on the first 20 principal components.

Clonal structure was determined using SCEVAN from inferred copy-number alteration profiles [21]. Differential expression analysis was conducted using the Mann–Whitney–Wilcoxon Gene Set Test (mww-GST), as previously described [64]. Genes with an adjusted p-value ≤0.01 (Benjamini–Hochberg correction) and an absolute log2 fold change ≥0.58 were considered significantly differentially expressed. Gene Set Enrichment Analysis (GSEA) of Gene Ontology terms was performed using ranked gene lists from each differential expression comparison using the clusterProfiler package (v3.3.6) [61].

In silico simulations of protein dynamics

The 3D structure of the extracellular region of Tie2 (receptor tyrosine kinase 2) has been built based on the structures of Ang1-bound Tie2 Ligand Binding Domain, LBD, complex (pdb ID: 4k0v) and the membrane-proximal three Tie2 Fibronectin-type (FN) domains (pdb ID: 5utk). Maestro suite [65] was employed to insert point mutation (S466I) and perform protein structural refinements; molecular dynamics simulation of the *wild-type* (*wt*) and mutant (S466I) protein were carried out using Gromacs 5.1.5 [66] by applying the Amber03 force field, following the same protocol described [67].

Two independent MD replicas of 100 ns simulation time in an NPT ensemble were run per system (*wt* and S466I). Gromacs routines, VMD [68] and Pymol [69] software were used to analyze and render simulations results. Electrostatic potential surface calculation was based on the APBS method—Adaptive Poisson–Boltzmann Solver [70].

Antibodies and reagents

The following primary antibodies were purchased from Cell Signaling Technology (CST; Danvers, MA): phospho-EGFR (Y1068; 3777), ID1 (23369), ID3 (9837), EGFR (C74B9; 2646), HA-Tag (6E2; 2367), GAPDH XP (5174) and α-Tubulin (05–829) were purchased from Millipore (Burlington, MA). Primary antibodies were diluted in Odyssey Blocking Buffer with 0.1% Tween 20 and incubated overnight with gentle shaking at 4 °C. IRDye 800CW secondary antibodies (LI-COR Biosciences, Lincoln, NE) were also diluted in Odyssey Blocking Buffer with 0.1% Tween 20 and incubated with membranes for 1 h at room temp with gentle shaking.

For use in in vivo and in vitro experiments, AbbVie (North Chicago, IL) provided EGFR-specific antibody ABT-806, isotype control antibody AB095, and ABT-414. All compounds were stored at −80 °C in single-use aliquots.

Cell culture

The primary GBM PDX lines GBM8 and GBM22 were acquired from the Mayo Clinic Brain Tumor Patient-Derived Xenograft National Resource [19]. Briefly, these cell lines were established from a patient surgical sample and maintained as a flank xenograft in immunodeficient mice. GBM8 and GBM22 flank tumors were resected, brought to single-cell suspension via mechanical dissociation, and then subsequently maintained as adherent cultures in DMEM supplemented with 10% fetal bovine serum for the studies herein.

Expression constructs

GBM22 cells expressing EGFR were made from plasmid WLZ-hygro-EGFR-as3 (a gift from Dr. Qi-Wen Fan, as in a previous study [71]). A plasmid containing the coding sequence of human TEK was obtained from GeneCopoeia (Rockville, MD; EX-L5239-Lv105). The TEK coding sequence was amplified by PCR and subcloned into pcDNA3 in frame with a C-terminal 3X HA epitope. The TEK-3XHA coding sequence was amplified and subcloned into the lentiviral vector pCDH-CMV-MCS-EF1a-GreenPuro (System Biosciences, Palo Alto, CA; CD513B-1) using the NEBuilder HiFi DNA Assembly kit (New England Biolabs, Ipswich, MA; E5520S). The

TEK S466I variant was generated using the QuikChange IISite-Directed MutagenesisKit (Agilent Technologies, Santa Clara, CA; 200,523) and the pCDH CMV TEK 3XHA GreenPuro clone as template. All alterations were confirmed by sequencing.

Western blot analysis

Monolayers of adherent cells were washed once with phosphate-buffered saline (PBS) containing 1 mmol/L phenylmethylsulfonylfluoride on ice and lysed in 1X RIPA buffer supplemented with 1X HALT protease and phosphatase inhibitors. Lysates were sonicated, and protein concentration was determined using BCA Assay with bovine serum albumin as a standard. Forty micrograms of total protein were loaded per lane and separated via a 4–12% gradient or 10% SDS-PAGE gel using the Novex Surelock Mini electrophoresis unit. Protein was transferred to a nitrocellulose membrane using the BioRad fast transfer system. Membranes were briefly rinsed with diH2O and blocked for at least 30 minutes at room temperature with Odyssey Blocking Buffer (LI-COR). Primary and secondary antibodies were diluted in Odyssey Blocking Buffer with 0.1% Tween-20. Protein bands were then detected with the Odyssey CLx Near-Infrared (NIR) Western Blot Detection System (LI-COR Biosciences).

Cell viability assay

Cell viability was assessed using the CellTiter-Glo Luminescent Cell Viability Assay (Promega, Madison, WI; G7570) according to the manufacturer's instructions. Reagent was reconstituted and aliquoted at 100% concentration for storage at −20 °C. On the day of assay, aliquots were thawed at 37 °C and diluted 1:1 in PBS prior to use. Cells were seeded at a density of 4,000 cells per well in 90 µL of complete growth medium in white solid-bottom 96-well plates (Corning, Corning NY). After 24 hours, cells were treated with 10 µg/mL of ABT-095 or ABT-414 in 10 µL of medium (final volume 100 µL). MMAF viability was measured 72 hours post-treatment, while ABT-414-treated cells were assayed 120 hours post-dose. At endpoint, 50 µL of CellTiter-Glo reagent (1:1 diluted with PBS) was added to each well and plates were incubated at 37 °C for 30 minutes. Luminescence was measured using a BioTek Cytation5 multimode plate reader.

Flow cytometric analysis of EGFR cell surface expression

GBM8 cells, GBM8 cells expressing WT TEK, and GBM8 cells expressing TEK S466I were harvested with 0.02% EDTA in Ca^{2+} and Mg^{2+}-free PBS and washed three times with PBS containing 0.5% BSA. Cells were fixed with ice-cold 4% paraformaldehyde in PBS for 10 min, washed, and incubated for 1 h with a PE-conjugated anti-EGFR monoclonal antibody (BD Biosciences, Franklin Lakes, NJ; 555,997) or a PE-conjugated mouse IgG2b isotype control antibody (BD Biosciences; 555,743). Samples were run on the BD Biosciences FACSCelesta System (BD Biosciences), and the data were analyzed using BD FACSDiva software (BD Biosciences).

Quantitative PCR

GBM8 cells were grown as described above. RNA was harvested using an RNAeasy Mini Kit (Qiagen, 74,104). cDNA conversion was accomplished using the iScript cDNA Synthesis Kit according to manufacturer recommendations (Bio-Rad, Hercules, CA; 1,708,891). Quantitative polymerase chain reaction (qPCR) was performed using Taqman Fast Advanced Master Mix according to manufacturer instructions (Applied Biosystems, Waltham, MA; 4,444,963). The following primers were used: 18S (ThermoFisher Scientific, Waltham, MA; 4,331,182 Hs99999901_s1), EGFR (ThermoFisher Scientific, 4,331,182 Hs06634166_s1), and TEK (ThermoFisher Scientific, 4,331,182 Hs00945150_m1).

Activity-based protein profiling

ABPP experiments were carried out using Pierce® Kinase Enrichment Kits and ActivX® ATP Probes (ThermoFisher Scientific; PI88310), according to the manufacturers' instructions and as previously published [71]. Briefly, cells were sonicated (3 cycles of 30 seconds at 1-minute intervals using a pulse of 50% duty cycle on VCX130 Vibra-Cell TM, Sonics) in 400 µL of lysis buffer with 4 µL of Halt™ phosphatase and protease inhibitor cocktail (ThermoFisher Scientific; 78,440). Lysates were cleared by centrifugation at 14,000 ×g for 20 minutes at 4 °C. Clarified lysates were desalted using 7K MWCO Zeba Spin Desalting Columns (ThermoFisher Scientific; 89,877). Protein concentrations were estimated using BCA assay, and a total of 1 mg of protein from each lysate was prepared for labeling, enrichment, and LC-MS/MS analysis. Protein extracts were sequentially incubated with 20 mM $MgCl_2$ and 10 µM DesThioBiotinylated (DBT)-ATP probes for 10 minutes each. Following labeling, proteins were denatured in 10 M urea, reduced with 5 mM DTT and alkylated with 40 mM iodoacetamide. Following second round of desalting (7K MWCO Zeba spin columns), proteins were digested overnight using trypsin (1:50 enzyme-to-substrate ratio) at 37 °C. DBT-labeled peptides were captured by incubating the digests with 50 µL of high-capacity streptavidin beads for 1 hour. Beads were washed sequentially three times with lysis buffer, PBS, and HPLC-grade water; bound peptides were eluted by addition of aqueous 50% acetonitrile with 0.1% trifluoroacetic acid (TFA). The eluted peptides were vacuum-concentrated and resuspended in loading solvent (98% water, 2% acetonitrile, 0.1% formic acid) for LC-MS/MS analysis.

Liquid chromatography and mass spectrometry

LC-MS/MS data were acquired on a U3000 RSLCnano liquid chromatography system coupled to an Orbitrap Eclipse mass spectrometer with a FAIMS Pro device (ThermoFisher Scientific). Peptides were directly loaded on a 50 cm C18 column (EasySpray ES903, 2 µm particle size and 75 µm ID) and separated using a 2-hour LC-method at a flow-rate of 300 nL/min. Using a duty cycle of 1 second per FAIMS compensation voltage (–40/-60/-80), data was acquired with the following settings: spray voltage of 2100 V, capillary temperature of 305 °C, MS1 scan in the Orbitrap at a resolution of 120K at 200 m/z, scan range of 375–1575 m/z and AGC target of 4E5 and maximum ion injection time of 50 ms. Data-dependent MS2 scans were carried out using High Energy Collision (HCD) dissociation of top abundant peaks and detection in the orbitrap at 30K resolution with the following settings: quadrupole isolation mode enabled, isolation window at 1.6 m/z, AGC target of 5E4 with maximum ion injection time of 35 ms and 32% NCE. Dynamic exclusion was set to 60 seconds.

Protein identification and quantification

Protein identification and label free relative quantification was performed using the Mascot search engine (v2.7) in Proteome Discoverer 2.4 (ThermoFisher Scientific) on a human UniProt/SwissProt database (downloaded May 2020) with the following parameters: trypsin cleavage rules, up to 2 missed cleavages, cysteine carbamidomethylation set as fixed modification, dynamic modification allowed were desthiobiotinylation of lysine residues, methionine oxidation and N-terminal acetylation. A 1% PSM and peptide false-discovery-rate was applied, calculated via Percolator. Peptide and protein abundances were normalized by variance stabilizing normalization via the vsn package in R v3.6.0. Peptide-level differential analysis was conducted using ANOVA, followed by a Tukey post-hoc for multiple testing correction. Kinase-substrate associations were annotated from the Uniprot database.

Statistical analysis

One-way analysis of variance (ANOVA) was used to determine whether normalized cell viability measurements. Tukey's multiple comparisons test was used to correct for multiple comparisons. p-values < 0.05 were considered statistically significant. All statistical tests were completed in GraphPad Prism.

Abbreviations

ADC	Antibody drug conjugate
AXL	Axl receptor tyrosine kinase
BMP	Bone morphogenetic protein
BRAF	B-Raf proto-oncogene serine/threonine kinase
CAMK2D	Calcium/calmodulin dependent protein kinase II delta
CDKN2A	Cyclin-dependent kinase inhibitor 2A
CIT	Citron-kinase
EGF	Epidermal growth factor
EGFR	Epidermal growth factor receptor
EPHB2	Ephrin type-B receptor 2
FGFR1	Fibroblast growth factor receptor 1
FLT-3	Fms-like tyrosine kinase
GBM	Glioblastoma
HAVCR1	Hepatitis A virus cellular receptor 1
IDH	Isocitrate dehydrogenase
ID1	Inhibitor of DNA binding 1
ID3	Inhibitor of DNA binding 3
KIT	Kit proto-oncogene receptor tyrosine kinase
MD	Molecular dynamics
MER	MER proto-oncogene tyrosine kinase
MET	MET proto-oncogene receptor tyrosine kinase; hepatocyte growth factor receptor
MMAF	Monomethyl auristatin F
PDPK1	3-phosphoinositide dependent protein kinase 1
PDGFRB	Platelet derived growth factor receptor beta
PI3K	Phosphoinositide 3-kinase
PLXNA2	Plexin A2
PSD2	Phosphatidylserine decarboxylase 2
PDX	Patient derived xenograft
RET	Ret proto-oncogene
RTK	Receptor tyrosine kinase
SRC	Proto-oncogene tyrosine-protein kinase Src
SRPRA	Signal recognition particle receptor subunit alpha
TEK	TEK receptor tyrosine kinase
TP53	Tumor protein p53
TRKB	Neurotrophic tyrosine kinase receptor type 2
TYRO3	Protein tyrosine kinase 3
UMAP	Uniform manifold for approximation and projection
VEGFR	Vascular endothelial growth factor receptor
WT	Wild type

Supplementary Information

The online version contains supplementary material available at https://doi.org/10.1186/s12967-025-07216-5.

Supplementary Material 1

Supplementary Material 2

Supplementary Material 3

Supplementary Material 4

Supplementary Material 5

Acknowledgements

Not applicable

Author contributions

MRB, TMRN, PP, AI, JNS, JCL and NT conceived the study. MB, CS, DG, RS, JK, BMM, KP, SJ, and BR performed most molecular and animal experiments and technical supports. TMRN, FPC, KGM, FD, AP performed the computational and bioinformatic analyses. MRB, TMRN, SPFE, AI, AP, JNS, MC, and NLT wrote the manuscript. All authors read and approved the manuscript.

Funding

The work is funded by U54CA210180 (NLT, JNS) and R01CA271431 (NLT). We also acknowledge the support of the Integrated Mass Spectrometry Shared Resource at the City of Hope Comprehensive Cancer Center supported by the National Cancer Institute of the National Institutes of Health under award number P30CA33572 (PP). Support also provided by Mayo Clinic (NLT, JNS) and the William H. Donnor Professorship (JNS).

Data availability

Genomic data will be uploaded into GenBank and proteomics data will be uploaded to PRIDE upon manuscript acceptance.

Declarations

Ethics approval and consent to participate
All animal studies were in accordance with the guidelines of and approved by the Institutional Animal Care and Use Committee (IACUC) of Mayo Clinic.

Consent for publication
All authors give consent for the publication of the manuscript in Journal of Experimental & Clinical Cancer Research.

Competing interests
The authors declare no competing interests.

Author details
[1]Department of Cancer Biology, Mayo Clinic Arizona, 5777 E. Mayo Blvd., IERB-3-504A, Phoenix, Arizona 85054, USA
[2]Department of Neurological Surgery, Mayo Clinic Arizona, 5777 E. Mayo Blvd., IERB-3-504A, Phoenix, Arizona 85054, USA
[3]Mayo Clinic Alix School of Medicine Arizona, Scottsdale, Arizona, USA
[4]Mayo Clinic Graduate School of Biomedical Sciences, Mayo Clinic, Rochester, MN, USA
[5]Department of Public Health Sciences, Miller School of Medicine, University of Miami, Miami, FL, USA
[6]Sylvester Comprehensive Cancer Center, Miller School of Medicine, University of Miami, Miami, FL, USA
[7]BIOGEM Institute of Molecular Biology and Genetics, Ariano Irpino, Italy
[8]Early Detection and Prevention Division, Translational Genomics Research Institute, Phoenix, Arizona, USA
[9]Integrated Mass Spectrometry Shared Resource, City of Hope Comprehensive Cancer Center, Duarte, California, USA
[10]Department of Neurological Surgery, Sylvester Comprehensive Cancer Center, Miller School of Medicine, University of Miami, Miami, FL, USA
[11]Department of Radiation Oncology, Mayo Clinic, Rochester, MN, USA
[12]Department of Hematology and Oncology, Mayo Clinic Arizona, Phoenix, Arizona, USA
[13]Institute of Biostructure and Bioimaging, Department of Biomedical Sciences, National Research Council (CNR), Naples, Italy

Received: 12 August 2025 / Accepted: 21 September 2025
Published online: 21 October 2025

References

1. Srivastava R, Dodda M, Zou H, Li X, Hu B. Tumor niches: perspectives for targeted therapies in Glioblastoma. Antioxid Redox Signal. 2023;39:904–22
2. Qazi MA, Vora P, Venugopal C, Sidhu SS, Moffat J, Swanton C, Singh SK. Intratumoral heterogeneity: Pathways to treatment resistance and relapse in human glioblastoma. Ann Oncol. 2017;28:1448–56
3. Fukushima CM, de Groot J. Updates for newly diagnosed and recurrent glioblastoma: A review of recent clinical trials. Curr Opin in Neurol. 2024;37:666–71
4. Brennan CW, Verhaak RG, McKenna A, Campos B, Noushmehr H, Salama SR, Zheng S, Chakravarty D, Sanborn JZ, Berman SH, et al. The somatic genomic landscape of glioblastoma. Cell. 2013;155:462–77
5. Thiessen B, Stewart C, Tsao M, Kamel-Reid S, Schaiquevich P, Mason W, Easaw J, Belanger K, Forsyth P, McIntosh L, Eisenhauer E. A phase I/II trial of GW572016 (lapatinib) in recurrent glioblastoma multiforme: Clinical outcomes, pharmacokinetics and molecular correlation. Cancer chemother-pharmacol. 2010;65:353–61
6. Uhm JH, Ballman KV, Wu W, Giannini C, Krauss JC, Buckner JC, James CD, Scheithauer BW, Behrens RJ, Flynn PJ, et al. Phase II evaluation of gefitinib in patients with newly diagnosed grade 4 astrocytoma: Mayo/North central cancer treatment group study N0074. Int J Radiat Oncol Biol Phys. 2011;80:347–53
7. van den Bent Mj, Brandes AA, Rampling R, Kouwenhoven MC, Kros JM, Carpentier AF, Clement PM, Frenay M, Campone M, Baurain JF, et al. Randomized phase II trial of erlotinib versus temozolomide or carmustine in recurrent glioblastoma: EORTC brain tumor group study 26034. J Clin Oncol. 2009;27:1268–74
8. Hu LS, D'Angelo F, Weiskittel TM, Caruso FP, Fortin Ensign SP, Blomquist MR, Flick MJ, Wang L, Sereduk CP, Meng-Lin K, et al. Integrated molecular and multiparametric MRI mapping of high-grade glioma identifies regional biologic signatures. Nat Commun. 2023;14:6066
9. Orellana L, Thorne AH, Lema R, Gustavsson J, Parisian AD, Hospital A, Cordeiro TN, Bernado P, Scott AM, Brun-Heath I, et al. Oncogenic mutations at the EGFR ectodomain structurally converge to remove a steric hindrance on a kinase-coupled cryptic epitope. Proc Natl Acad Sci U S A. 2019;116:10009–18
10. Jain S, Griffith JI, Porath KA, Rathi S, Le J, Pasa TI, Decker PA, Gupta SK, Hu Z, Carlson BL, et al. Bystander effects, pharmacokinetics, and linker-payload stability of EGFR-Targeting antibody-drug conjugates losatuxizumab vedotin and depatux-M in Glioblastoma models. Clin Cancer Res. 2024;30:3287–97
11. Phillips AC, Boghaert ER, Vaidya KS, Mitten MJ, Norvell S, Falls HD, DeVries PJ, Cheng D, Meulbroek JA, Buchanan FG, et al. ABT-414, an antibody-Drug conjugate targeting a tumor-selective EGFR epitope. Mol cancerther. 2016;15:661–69
12. Rock BM, Tometsko ME, Patel SK, Hamblett KJ, Fanslow WC, Rock DA. Intracellular catabolism of an antibody drug conjugate with a noncleavable linker. Drug Metab Dispos. 2015;43:1341–44
13. Lassman AB, Pugh SL, Wang TJC, Aldape K, Gan HK, Preusser M, Vogelbaum MA, Sulman EP, Won M, Zhang P, et al. Depatuxizumab mafodotin in EGFR-amplified newly diagnosed glioblastoma: a phase III randomized clinical trial. NeuroOncol. 2023;25:339–50
14. Marin BM, Porath KA, Jain S, Kim M, Conage-Pough JE, Oh JH, Miller CL, Talele S, Kitange GJ, Tian S, et al. Heterogeneous delivery across the blood-brain barrier limits the efficacy of an EGFR-targeting antibody drug conjugate in glioblastoma. NeuroOncol. 2021;23:2042–53
15. Loganzo F, Tan X, Sung M, Jin G, Myers JS, Melamud E, Wang F, Diesl V, Follettie MT, Musto S, et al. Tumor cells chronically treated with a trastuzumab-maytansinoid antibody-drug conjugate develop varied resistance mechanisms but respond to alternate treatments. Mol cancer ther. 2015;14:952–63
16. Niola F, Zhao X, Singh D, Sullivan R, Castano A, Verrico A, Zoppoli P, Friedmann-Morvinski D, Sulman E, Barrett L, et al. Mesenchymal high-grade glioma is maintained by the ID-RAP1 axis. J. clin.Invest. 2013;123:405–17
17. Soroceanu L, Murase R, Limbad C, Singer E, Allison J, Adrados I, Kawamura R, Pakdel A, Fukuyo Y, Nguyen D, et al. Id-1 is a key transcriptional regulator of glioblastoma aggressiveness and a novel therapeutic target. Cancer Res. 2013;73:1559–69
18. Lasorella A, Benezra R, Iavarone A. The ID proteins: Master regulators of cancer stem cells and tumour aggressiveness. Nat Rev Cancer. 2014;14:77–91
19. Vaubel RA, Tian S, Remonde D, Schroeder MA, Mladek AC, Kitange GJ, Caron A, Kollmeyer TM, Grove R, Peng S, et al. Genomic and phenotypic characterization of a broad panel of patient-derived xenografts reflects the diversity of Glioblastoma. Clin Cancer Res. 2020;26:1094–104
20. Sachdeva R, Wu M, Smiljanic S, Kaskun O, Ghannad-Zadeh K, Celebre A, Isaev K, Morrissy AS, Guan J, Tong J, et al. ID1 is critical for tumorigenesis and regulates chemoresistance in Glioblastoma. CancerRes. 2019;79:4057–71
21. De Falco A, Caruso F, Su XD, Iavarone A, Ceccarelli M. A variational algorithm to detect the clonal copy number substructure of tumors from scRNA-seq data. Nat Commun. 2023;14:1074
22. Suva ML, Rheinbay E, Gillespie SM, Patel AP, Wakimoto H, Rabkin SD, Riggi N, Chi AS, Cahill DP, Nahed BV, et al. Reconstructing and reprogramming the tumor-propagating potential of glioblastoma stem-like cells. Cell. 2014;157:580–94
23. Deshors P, Toulas C, Arnauduc F, Malric L, Siegfried A, Nicaise Y, Lemarie A, Larrieu D, Tosolini M, Cohen-Jonathan Moyal E, et al. Ionizing radiation induces endothelial transdifferentiation of glioblastoma stem-like cells through the Tie2 signaling pathway. Cell Deathdis. 2019;10:816
24. Duran CL, Borriello L, Karagiannis GS, Entenberg D, Oktay MH, Condeelis JS. Targeting Tie2 in the tumor microenvironment: from angiogenesis to dissemination. Cancers (basel). 2021;13
25. Ye K, Li J, Li X, Chang S, Zhang Z. Ang1/Tie2 induces cell proliferation and migration in human papillary thyroid carcinoma via the PI3K/AKT pathway. OncolLett. 2018;15:1313–18
26. Li X, Martinez-Ledesma E, Zhang C, Gao F, Zheng S, Ding J, Wu S, Nguyen N, Clifford SC, Wen PY, et al. Tie2-FGFR1 interaction induces adaptive PI3K inhibitor resistance by upregulating aurora A/PLK1/CDK1 signaling in Glioblastoma. Cancer Res. 2019;79:5088–101
27. Iegiani G, Di Cunto F, Pallavicini G. Inhibiting microcephaly genes as alternative to microtubule targeting agents to treat brain tumors. Cell deathdis. 2021;12:956
28. Jungas T, Perchey RT, Fawal M, Callot C, Froment C, Burlet-Schiltz O, Besson A, Davy A. Eph-mediated tyrosine phosphorylation of citron kinase controls abscission. The J Cellbiol. 2016;214:555–69

29. Jin X, Yin J, Kim SH, Sohn YW, Beck S, Lim YC, Nam DH, Choi YJ, Kim H. EGFR-AKT-Smad signaling promotes formation of glioma stem-like cells and tumor angiogenesis by ID3-driven cytokine induction. CancerRes. 2011;71:7125–34
30. Jun HJ, Acquaviva J, Chi D, Lessard J, Zhu H, Woolfenden S, Bronson RT, Pfannl R, White F, Housman DE, et al. Acquired MET expression confers resistance to EGFR inhibition in a mouse model of glioblastoma multiforme. Oncogene. 2012;31:3039–50
31. Akhavan D, Pourzia AL, Nourian AA, Williams KJ, Nathanson D, Babic I, Villa GR, Tanaka K, Nael A, Yang H, et al. De-repression of PDGFRbeta transcription promotes acquired resistance to EGFR tyrosine kinase inhibitors in glioblastoma patients. Cancer Discov. 2013;3:534–47
32. Harney AS, Karagiannis GS, Pignatelli J, Smith BD, Kadioglu E, Wise SC, Hood MM, Kaufman MD, Leary CB, Lu WP, et al. The selective Tie2 inhibitor rebastinib blocks recruitment and function of Tie2(Hi) macrophages in breast cancer and pancreatic neuroendocrine tumors. Mol Can Certher. 2017;16:2486–501
33. Jóri B, Vössing C, Pirngruber J, Willing EM, Arndt K, Falk M, Tiemann M, Heukamp LC, Hoffknecht P. The combined therapy of Cabozantinib, crizotinib, and osimertinib in a lung cancer patient with acquired MET amplification and resistance mutations. Curr Oncol. 2023;30:8805–14
34. Desilets A, Pfister DG, Stein S, Wong W, Sherman EJ, Fetten J, Hung TKW, Kriplani A, Dunn LA, Ho AL, Michel LS. A phase 1 study of concurrent cabozantinib and cetuximab in recurrent or metastatic head and neck squamous cell cancer. Oral Oncol. 2024;154:106861
35. Graves-Deal R, Bogatcheva G, Rehman S, Lu Y, Higginbotham JN, Singh B. Broad-spectrum receptor tyrosine kinase inhibitors overcome de novo and acquired modes of resistance to EGFR-targeted therapies in colorectal cancer. Oncotarget. 2019;10:1320–33
36. Wakelee HA, Gettinger S, Engelman J, Jänne PA, West H, Subramaniam DS, Leach J, Wax M, Yaron Y, Miles DR, Lara PN Jr. A phase Ib/II study of cabozantinib (XL184) with or without erlotinib in patients with non-small cell lung cancer. Cancer Chemother Pharmacol. 2017;79:923–32
37. Sobrino A, Phan DT, Datta R, Wang X, Hachey SJ, Romero-López M, Gratton E, Lee AP, George SC, Hughes CC. 3D microtumors in vitro supported by perfused vascular networks. SciRep. 2016;6:31589
38. Hu L, Shi W, Liu K, Ma D, Xin Q, Wang Z, Cao Y, Zhang G. EGFR bypass activation mediates acquired resistance to regorafenib in hepatocellular carcinoma. Front Med (Lausanne). 2024;11:1464610
39. Mehta M, Griffith J, Panneerselvam J, Babu A, Mani J, Herman T, Ramesh R, Munshi A. Regorafenib sensitizes human breast cancer cells to radiation by inhibiting multiple kinases and inducing DNA damage. Int J Radiat Biol. 2021;97:1109–20
40. Deshors P, Arnauduc F, Boëlle B, Cohen-Jonathan Moyal E, Courtade-Saïdi M, Evrard SM. Impact of regorafenib on endothelial transdifferentiation of Glioblastoma stem-like cells. Cancers (basel). 2022;14
41. Inoue K, Torimura T, Nakamura T, Iwamoto H, Masuda H, Abe M, Hashimoto O, Koga H, Ueno T, Yano H, Sata M. Vandetanib, an inhibitor of VEGF receptor-2 and EGF receptor, suppresses tumor development and improves prognosis of liver cancer in mice. Clin Cancer Res. 2012;18:3924–33
42. Arbab AS. Activation of alternative pathways of angiogenesis and involvement of stem cells following anti-angiogenesis treatment in glioma. Histol-Histopathol. 2012;27:549–57
43. Carlson BL, Pokorny JL, Schroeder MA, Sarkaria JN. Establishment, maintenance and in vitro and in vivo applications of primary human glioblastoma multiforme (GBM) xenograft models for translational biology studies and drug discovery. Curr Protoc Pharmacol. 2011;14::16
44. Conway T, Wazny J, Bromage A, Tymms M, Sooraj D, Williams ED, Beresford-Smith B. Xenome-a tool for classifying reads from xenograft samples. Bioinformatics. 2012;28:i172–178
45. Li H, Durbin R. Fast and accurate short read alignment with Burrows-Wheeler transform. Bioinformatics. 2009;25:1754–60
46. DePristo MA, Banks E, Poplin R, Garimella KV, Maguire JR, Hartl C, Philippakis AA, Del Angel G, Rivas MA, Hanna M, et al. A framework for variation discovery and genotyping using next-generation DNA sequencing data. NatGenet. 2011;43:491–98
47. Kendig KI, Baheti S, Bockol MA, Drucker TM, Hart SN, Heldenbrand JR, Hernaez M, Hudson ME, Kalmbach MT, Klee EW, et al. Sentieon DNASeq variant calling workflow demonstrates strong computational performance and accuracy. FrontGenet. 2019;10:736
48. Garrison E, Marth G. Haplotype-based variant detection from short-read sequencing. arxiv Prepr arxiv. 2012,1207–3907
49. Cibulskis K, Lawrence MS, Carter SL, Sivachenko A, Jaffe D, Sougnez C, Gabriel S, Meyerson M, Lander ES, Getz G. Sensitive detection of somatic point mutations in impure and heterogeneous cancer samples. NatBiotechnol. 2013;31:213–19
50. Koboldt DC, Zhang Q, Larson DE, Shen D, McLellan MD, Lin L, Miller CA, Mardis ER, Ding L, Wilson RK. VarScan, 2: Somatic mutation and copy number alteration discovery in cancer by exome sequencing. GenomeRes. 2012;22:568–76
51. Wang K, Li M, Hakonarson H. ANNOVAR: Functional annotation of genetic variants from high-throughput sequencing data. Nucleic acidsres. 2010;38:e164
52. Cingolani P, Platts A, le L W, Coon M, Nguyen T, Wang L, Land SJ, Lu X, Ruden DM. A program for annotating and predicting the effects of single nucleotide polymorphisms, SnpEff: SNPs in the genome of drosophila melanogaster strain w1118. 2012;6(2. Fly (Austin) 80–92
53. Adzhubei IA, Schmidt S, Peshkin L, Ramensky VE, Gerasimova A, Bork P, Kondrashov AS, Sunyaev SR. A method and server for predicting damaging missense mutations. Nat Methods. 2010;7:248–49
54. Ng PC, Henikoff S. Predicting deleterious amino acid substitutions. GenomeRes. 2001;11:863–74
55. Choi Y, Sims GE, Murphy S, Miller JR, Chan AP. Predicting the functional effect of amino acid substitutions and indels. PLoS One. 2012;7:e46688
56. Talevich E, Shain AH, Botton T, Bastian BC. Cnvkit: Genome-wide copy number detection and visualization from targeted DNA sequencing. PLoS ComputBiol. 2016;12:e1004873
57. Mermel CH, Schumacher SE, Hill B, Meyerson ML, Beroukhim R, Getz G. GISTIC2.0 facilitates sensitive and confident localization of the targets of focal somatic copy-number alteration in human cancers. GenomeBiol. 2011;12:R41
58. Dobin A, Davis CA, Schlesinger F, Drenkow J, Zaleski C, Jha S, Batut P, Chaisson M, Gingeras TR. STAR: ultrafast universal RNA-seq aligner. Bioinformatics. 2013;29:15–21
59. Liao Y, Smyth GK, Shi W. featureCounts: An efficient general purpose program for assigning sequence reads to genomic features. Bioinformatics. 2014;30:923–30
60. Risso D, Schwartz K, Sherlock G, Dudoit S. GC-content normalization for RNA-Seq data. BMCBioinf. 2011;12:480
61. Robinson MD, McCarthy DJ, Smyth GK. edgeR: A Bioconductor package for differential expression analysis of digital gene expression data. Bioinformatics. 2010;26:139–40
62. Cheloni S, Hillje R, Luzi L, Pelicci PG, Gatti E. XenoCell: Classification of cellular barcodes in single cell experiments from xenograft samples. BMC Med Genomics. 2021;14:34
63. Satija R, Farrell JA, Gennert D, Schier AF, Regev A. Spatial reconstruction of single-cell gene expression data. Nat Biotechnol. 2015;33:495–502
64. Frattini V, Pagnotta SM, Tala F Russo JJ Lee MV Garofano SB Zhang L Shi J P, Lewis G, et al. A metabolic function of FGFR3-TACC3 gene fusions in cancer. Nature. 2018;553:222–27
65. Maestro suite (from schrödinger suite molecular modelling package, version 2021-3)
66. Van Der Spoel D, Lindahl E, Hess B, Groenhof G, Mark AE, Berendsen HJ. GROMACS: fast, flexible, and free. J computchem. 2005;26:1701–18
67. Paladino A, D'Angelo F, Noviello TMR, Iavarone A, Ceccarelli M. Structural Model for recruitment of RIT1 to the LZTR1 E3 ligase: Evidences from an integrated computational approach. J Chem Inf Model. 2021;61:1875–88
68. Humphrey W, Dalke A, Schulten K. VMD: Visual molecular dynamics. J Mol Graph. 1996;14:33–38, 27–38
69. Schrödinger L, DeLano W. PyMOL. Available at: 2020. http://www.pymol.org/pymol
70. Jurrus E, Engel D, Star K, Monson K, Brandi J, Felberg LE, Brookes DH, Wilson L, Chen J, Liles K, et al. Improvements to the APBS biomolecular solvation software suite. ProteinSci. 2018;27:112–28
71. Blomquist MR, Eghlimi R, Beniwal A, Grief D, Nascari DG, Inge L, Sereduk CP, Tuncali S, Roos A, Inforzato H, et al. EGFRvIII confers sensitivity to Saracatinib in a STAT5-dependent manner in Glioblastoma. Int J molsci. 2024;25

Publisher's Note